

# Detection and Delineating of Hydrocarbon Contaminants by Using Time and Frequency Analysis of Ground Penetrating Radar

José Vicente Fuente

Research & Develop Department, Geozone Asesores SL, Bétera, Spain

Email: [j.fuente@gmail.com](mailto:j.fuente@gmail.com)

**How to cite this paper:** Fuente, J. V. (2021). Detection and Delineating of Hydrocarbon Contaminants by Using Time and Frequency Analysis of Ground Penetrating Radar. *Journal of Geoscience and Environment Protection*, 9, 35-56.

<https://doi.org/10.4236/gep.2021.912003>

**Received:** September 20, 2021

**Accepted:** December 12, 2021

**Published:** December 15, 2021

Copyright © 2021 by author(s) and Scientific Research Publishing Inc. This work is licensed under the Creative Commons Attribution International License (CC BY 4.0).

<http://creativecommons.org/licenses/by/4.0/>



Open Access

---

## Abstract

This paper provides the results of using ground penetrating radar (GPR) method to detect hydrocarbon products (diesel and gasoline) in a controlled lab test. The work addresses the environmental problem generated by the uncontrolled leakage of hydrocarbon products and the subsequent contamination of plumes in the subsoil. Most of the research proposes the geophysical techniques to evaluate the plumes but some controversial were discussed on how it affected the electrical and dielectric response depending on the excitation of the non-invasive method. The present work focuses on a comparative analysis of some signal attributes of the GPR traces to determine under what premises the detection is properly done. These signal attributes were from the time and frequency domain as attenuation coefficient, instantaneous amplitude and frequency have been considered to analyze three different soil samples. The laboratory tests consist of buried liquid (total hydrocarbon of petroleum, so called TPH) bags in the soil sample boxes reveal the range of target detection and consistency of data on the controlled test regarding the dielectric soil characterization and the delimiting position and depth. Instantaneous amplitude and time-frequency shift are revealed as promising signal attributes to accurate detection of the TPH presence. Numerical simulation data were also carried out to interpret the signal reflections on radargrams and to confirm experimental trends and the benefits of using the above signal attributes in time-frequency domain.

## Keywords

Time-Frequency Analysis, Instantaneous Amplitude, GPR Survey, Hydrocarbon Products

## 1. Introduction

The ground penetrating radar (GPR) is an electromagnetic prospecting method significantly spread out in geophysics to characterize the dielectric properties of the subsoil composition. Based on the electromagnetic wave propagation, most typical wave frequencies range between 10 - 2600 MHz providing a reasonable tool for inspection of hydrocarbon leakages and plumes formation in the subsoils. For various decades, oil spills are one of the most relevant environmental issues in soils contamination, especially in the industrial areas where installations, over and buried the ground, and deposits and tanks for storing hydrocarbon and chemical product and suppose a risk derivate against wrong tightness manipulation and transport. Hazard wastes would cause a contaminant problem for the local soil site but depending on the geological conditions, large extensions could be affected by the spill. In this sense, the contaminants could reach the watertable and migrate largely therefore geophysical investigation is imposed including vertical and lateral directions from the leakage point.

The hydrocarbon spills diffuse along the subsoil leaving the light density components in the vadose zone. These components are named by Light Non-aquose Phase Liquid (LNAPL) and can migrate until the fringe stripe with high water contents and the watertable. The dense components are named DNAPL and they can move down the watertable and migrate longer distances taking advantage of the underground water flow. This dynamic system has been studied by some research, but it can be found a deep investigation at doctoral research of J. McCallister (McCallister, 1994). There is a lot of experimental research that considers the soil electrical conductivity and dielectric properties. It is pointed out some illustrative research where induced polarization time or chargeability is proposed as a good indicator of hydrocarbon presence (Tejero & López, 2013), (Sogade et al., 2006) and (Deceuster & Kaufmann, 2012). Other efforts focused on joint both techniques ERT and GPR to verify the HTP presence (Hamzah et al., 2008).

Che-Alota et al. (Che-Alota et al., 2009) describe a conceptual model for bulk electrical conductivity and dielectric properties of the hydrocarbon mass and their changes along with the biodegradation actions.

Other researches have been focused on electrical tomography production assuming that the bulk electrical conductivity parameter could distinguish the contaminants or affected areas. Jianga et al. (Jiang et al., 2013) conclude that Wenner, Pole-Pole and Dipole-Dipole arrays are the most proper configurations against Schlumberger array. The seismic method has also been tested for that application, and some interesting advance is presented by Chen et al. (Chen et al., 2017) using time-frequency analysis for hydrocarbon detection in the tight sandstone reservoir.

The purpose of the research is to establish a testing procedure for the oil station based on geophysical testing and time-frequency analysis of ground penetration radar exploiting the interaction mechanisms of relaxation between LNAPL

and electromagnetic wave.

At this paper, it is presented controlled scaled tests and simulation of GPR measurements for buried bulk oil products (diesel and gasoline) in representative soil samples. So that, a complete literature review should be focused on advances in that specific topic using digital signal processing of GPR measurements and data simulation to understand the real behavior of signal and find signal attributes related to the changes. Some expectative comes from conference paper (Capozzoli et al., 2012) indicate that joint a decisive GPR acquisition data, data processing and contrast chemical test it is possible to achieve not only the zonification of affected areas but also the dissolved LNAPL presence at the vadose zone.

Conference Ground Penetrating Radar (Chen et al., 2012) presented how the frequency dependent time-lapse attributes could help to delineate the area polluted by LNAPL by PAHs (Polycyclic Aromatic Hydrocarbons) from hydrocarbon products when the detection shows very complex regarding the slight difference in the conductivity and dielectric values of the surrounding area. Nevertheless, there are other researches that indicate the complexity to achieve good results for that application (Golebiowski et al., 2010).

Consolidating the state-of-art, it seems that polarization of the hydrocarbon product when it is excited in-free phase and reacted by biodegradation process with the soil contour is different. The attributes of the response signal that contain information of the relaxation process are the most promising to detect the presence of HTP. Therefore the present work uses this kind of parameter to assess the addressed application.

Scaled laboratory tests observe different approaches to a better understanding of the signal response to the presence of hydrocarbons and soil samples under controlled dispositions. Mansi et al. (Mansi et al., 2017) found that tracking the amplitudes of the backwall reflection and propagation velocities is able to link this information to the presence of certain contaminants and water saturation. V. Perez-Gracia (Pérez-Gracia, 2001) shows in Chapter 6 of her doctoral research how influences the dielectric constant with other parameters humidity and porosity and signal attributes as the centered frequency of GPR pulse excitation. In the same way, O. Shamir et al. (Shamir et al., 2018) and Moreno et al. (Moreno & Montes, 2003) found relationships between conductivity and dielectric permittivity and water content and porosity for agricultural soils and sandy soils respectively.

Other research line addressed to clarify the response of electromagnetic wave interacting with LNAPL is the numerical simulation of radar profiles modeling different and designed strategic scenarios (Carcione & Seriani, 2000). In this sense, the software as GPR-Sim<sup>®</sup>, GPRMax<sup>®</sup> (Wijewardana et al., 2012) and ReflexW<sup>®</sup> are dedicated to simulate the radargram response for wide range of scenarios based on Finite Difference Time Domain (FDTD) or AVO techniques.

Marcak et al. (Marcak & Gołębiowski, 2008) found that some curve attributes of the calculated power spectra on simulated traces could be a useful technique to reveal the presence of LNAPL even when the changes on velocity are very small while L. Orlando (Orlando, 2002) put on the light the useful technique of complex trace (instantaneous amplitude and phase) to get more sensitive to the LNAPL detection.

The monitoring approach, considering the dynamic system formed by the porous media containing hydrocarbon contaminants with its phases vapor and liquid, requires studies including the variable time for monitoring an affected area. This is required before the implementation of remediation techniques of the soil. By the other hand, GPR numerical simulations and real on-site testing with further analysis considering signal attributes as power spectra envelope and instantaneous amplitude have provided good results for the LNAPL detection at real scenarios.

In this paper, the research is addressed to find evidence of the spectral changes of the GPR traces that contain non-mixed hydrocarbon products (diesel and gasoline) in three different samples. Scaled laboratory test will be complemented with numerical simulation.

After this literature review to approach the reader to the specific topic, it will be shown the representative soil samples preparation and characterization and the main features of the GPR equipment used by the scaled experiments. It is described the numerical simulation workflow and the main signal attributes that will be used to detect and locate the hydrocarbon presence. The following section shows the results structured in two round tests. The first round involves only soil sample characterization while the round 2 involves hydrocarbon samples as it will be described and the comparison with the numerical simulation of GPR traces to observed in which conditions and with which signal attributes, the detection and location are produced. The discussion section summarizes the main achievements from the initial hypothesis.

## **2. Materials and Methods**

### **2.1. Materials Preparation and Characterization**

Some representative soil samples and hydrocarbon products have been prepared and tested by GPR pulse/echo methodology. The three soil samples were a loamy soil with coarse aggregates or gravels (Soil1, S1); a red clay soil with fine particles passing 4 mm (Soil2, S2) and the third was a washed sand passing 2 mm (Soil3, S3). Three wooden box were built of 60 × 60 × 50 cm, to confine the soil samples and eventually some targeted liquid hydrocarbon bags (LHB) to produce some controlled experiments to observe if the detection and sizing of the LHB is done. The targeted TPH consist of a 10 × 6 cm of plastic bags (if empty) filled with two type of combustible diesel and gasoline were used during the experimentation acquiring a shape of ellipsoidal cylinder with a shape of crushed cylinder of 3 cm

of radius (when are full) at the propagation pathway.

Two main testing rounds have been performed as follows: a) round 1: involving three different frequencies and three thickness of soil (S1, S2, S3) close to T1 = 10, T2 = 20 and T3 = 30 cm. Also, it was used two buried cylindrical tubes to generate hyperbolic strong reflection and fit their curve to obtain wave velocity for that specific soil sample, b) round 2: measuring with the high working frequency (HWF) and both types of the buried bags of the combustible products (LHB) as a targets to be detected and do further analysis.

The physical characterization of soils comprises the apparent density  $\rho_{app}$ , the water connected porosity and the water content (WC) or humidity of a representative portion of 0.018 m<sup>3</sup> following the UNE 103-301-94 (Tomás et al., 2013). Both parameters affect to the electromagnetic interaction of the sample and the broadband excitation pulse. Using the dry, water saturated and hydros-tatic weight could be obtained the abovementioned physical parameters.

The characterization tests of each round were performed with 3 weeks of delay and characterization parameters are shown in Table 1. The first-round (round 1) few days after the sample reception and the second-round test (round 2) three weeks later stored at the laboratory facilities. It could be observed while clay sample S2 remain more or less the same range of parameters while the sandy and loam soil have shown weathering process and became drier than round 1. The observed changes would be correlated by the dielectric changes and also how the working or center frequency and thickness affect to the electromagnetic characterization according to the bibliography.

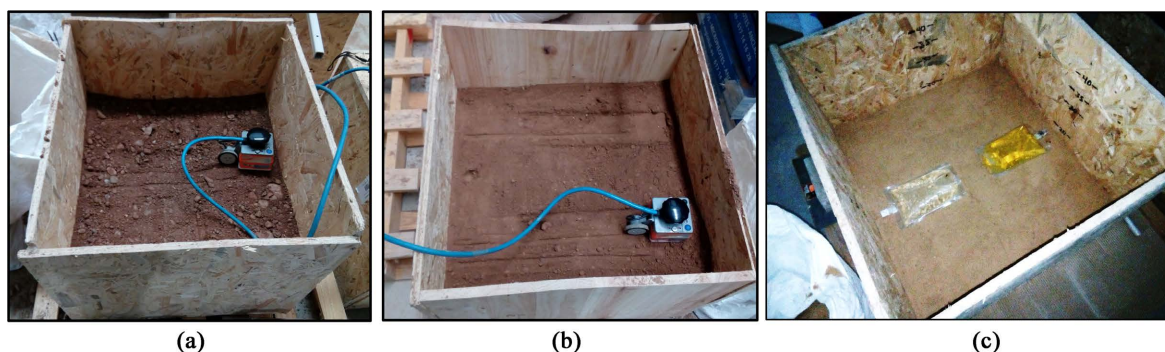


**Figure 1.** Pictures of the 3 wooden boxes with soil samples at different thickness: (a) Loam soil with coarse gravels with T1; (b) Red clay and (S2) with T2; (c) Washed sand (S3) with LHB bags placed to be buried are shown.

**Table 1.** Soil samples characterization.

Rounds Parameters/samples	Round 1			Round2		
	S1	S2	S3	S1	S2	S3
$\rho_{app}$ (g/cm <sup>3</sup> )	2.14	1.62	1.99	2.01	1.63	1.95
Porosity (%)	0.51	0.48	0.35	0.55	0.51	0.50
WC (%)	24.6	15.1	18.6	19.4	12.8	12.6

## 2.2. GPR Equipment and Type of Measurements

The GPR equipment used was the SIR3000 of GSSI® and the three working frequencies were excited by using the following antennas: a) The 270 MHz nominal frequency, model 5104 and shadow of  $44.5 \times 44.5$  cm and 3.6 ns pulse duration; b) The 900 MHz, model 3101,  $33 \times 18$  cm and 1.9 ns pulse duration; c) The antenna PALM 2000 GHz nominal frequency was equipped with odometers for non-static profiles and a shadow area of  $10.4 \times 9.2$  cm and a 0.44 ns of pulse duration.

According to the work of IEEE Xplore Conference Paper (Rial et al., 2007), the vertical and lateral resolution of the electromagnetic beam are related with the wavelength in the materials. Both resolutions are the minimum distance for two points to be separately observed or discriminated giving the vertical resolution by  $\Delta v$  and the horizontal resolution  $R_{hor}$  as the radius of the shadow cone radiation at specific depth. Next **Table 2** provides some actual values for a pulse excitation of GSSI SIR3000 and antennas used, for an averaged dielectric constant  $\epsilon_r$  of 8 and 200 mm of depth.

The GPR measurements focus the dielectric permittivity characterization and permit the coherence observance with related parameters and material conditions. The antennas with low and medium frequency were used with static measurements or profiles and the Palm antenna (HWF) of 2 GHz was used to obtain GPR traces by antenna linear displacement around 50 cm of length over the top of the sample. The HWF was also used to pulse/eco measurements of combustible bags before they were buried into the soil samples, exerting the right pressure to replicate test conditions and fix the thickness (see **Figure 2(d)**).

Round 1: dielectric constant vs soil thickness.

The three thickness around 10, 20 and 30 cm was considered to observe possible discrepancies of the dielectric constant  $\epsilon_r$  and wave or phase velocity that are related by a simple equation valid for typical non-dispersive soils (dry soils, non-magnetic and energy loss-less behaviors):

$$v = \frac{300}{\sqrt{\epsilon_r}} \quad (1)$$

with velocity the  $v$  expressed in mm/ns and the dielectric constant being non-dimensional.

For each thickness  $T_b$  the soil samples Si were measured by the three frequencies to observe the possible shifts or dependence between thicknesses, working

**Table 2.** Vertical and lateral resolution of used antennas for a giving depth and  $\epsilon_r$ .

Resolutions	Working frequencies		
	270 MHz	900 MHz	2000 MHz
$\Delta_v$ (mm)	98	29	13
$R_{hor}$ (mm)	330	27	16

frequency and soil type in terms of dielectric behavior. These working frequencies were selected ranging their diverse depth penetration and resolution according to the box sizes and further test at the actual sites. The low frequency of 270 MHz reaches until 6 - 7 meters in non-saturated soil, allowing the survey until water table in most cases. The medium frequency allows a vertical high resolution for the first meter and the 2 GHz antenna permits the highest vertical and lateral accuracy so that it was intensively used in the characterization testing rounds of this work.

First measures allow the velocity determination by hyperbolic fitting in two cylindrical PVC and aluminum tubes using the highest frequency (see **Figure 2(a)**). Two static measurements of 270 and 900 MHz by each thickness (see **Figure 2(b)**, **Figure 2(c)**) and two cross perpendicular profiles using 2 GHz antenna was used for each thickness and soil sample (see **Figure 1(a)**, **Figure 1(b)**).

Round 2: dielectric constant evolution and LHB characterization.

With buried combustible bags, three different types of measurements were performed: i) Crossing transversally both diesel and gasoline bags; ii) Crossing longitudinally diesel bag and iii) crossing longitudinally gasoline bag.

These controlled experiments allow to assess the dielectric changes when soil conditions vary from round 1 to round 2 conditions and to find which GPR signal attributes could be used to detect and to size the hydrocarbon presence and its occupied volume. Also, the expected dielectric permittivity (or velocity) variations according to the WC and open porosity changes will provide reliability to undertake large GPR survey at field in order to work on an effective testing procedure in further research stages.

### 2.3. Numerical Simulations

The objective of the numerical simulation is obtaining synthetic radargrams of controlled scenarios and extract the expected spectral signal attributes. In that case, the complex dielectric permittivity, and related parameters as feasible to assess the detection and size the LHB targets. The dc-electrical conductivity of

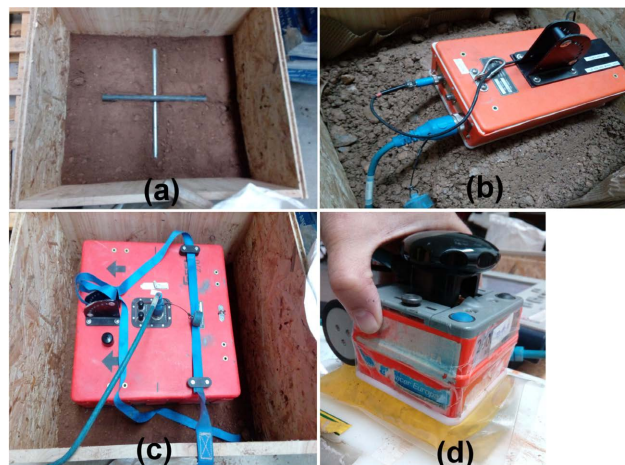


**Figure 2.** Pictures of the 4 types of GPR measurements described above.

each soil sample, the complex dielectric constant ( $\epsilon_{real}$  and  $\epsilon_{imag}$ ) and shape of wavelet have been used as inputs of the model for the round 2. In that section, the workflow of the GPR-Sim<sup>®</sup> software simulation is shown in **Figure 3**.

The synthetic radargrams could be also processed to extract the theoretical signal attributes. Observing the deviations between experimental and synthetic radargrams is a way to understand the usefulness of the lab-scale replication and modeling. This was also used to identify cross reflections below the backwall echo coming from lateral wall of the container.

### 2.4. Signal Processing

The results of GPR detection are commonly expressed in the format of GPR 2D profiles. The analysis of geo-radar sections should reveal the geometry, nature and type of contained objects and eventually layers. These GPR 2D profiles are the radargrams and could be considered as input for further processing routines and variables (signal attributes) for further correlation. Also, some other parameters can be extracted from a single trace that belongs to a radargram.

The digital signal processing deals with the parameters extraction of the actual

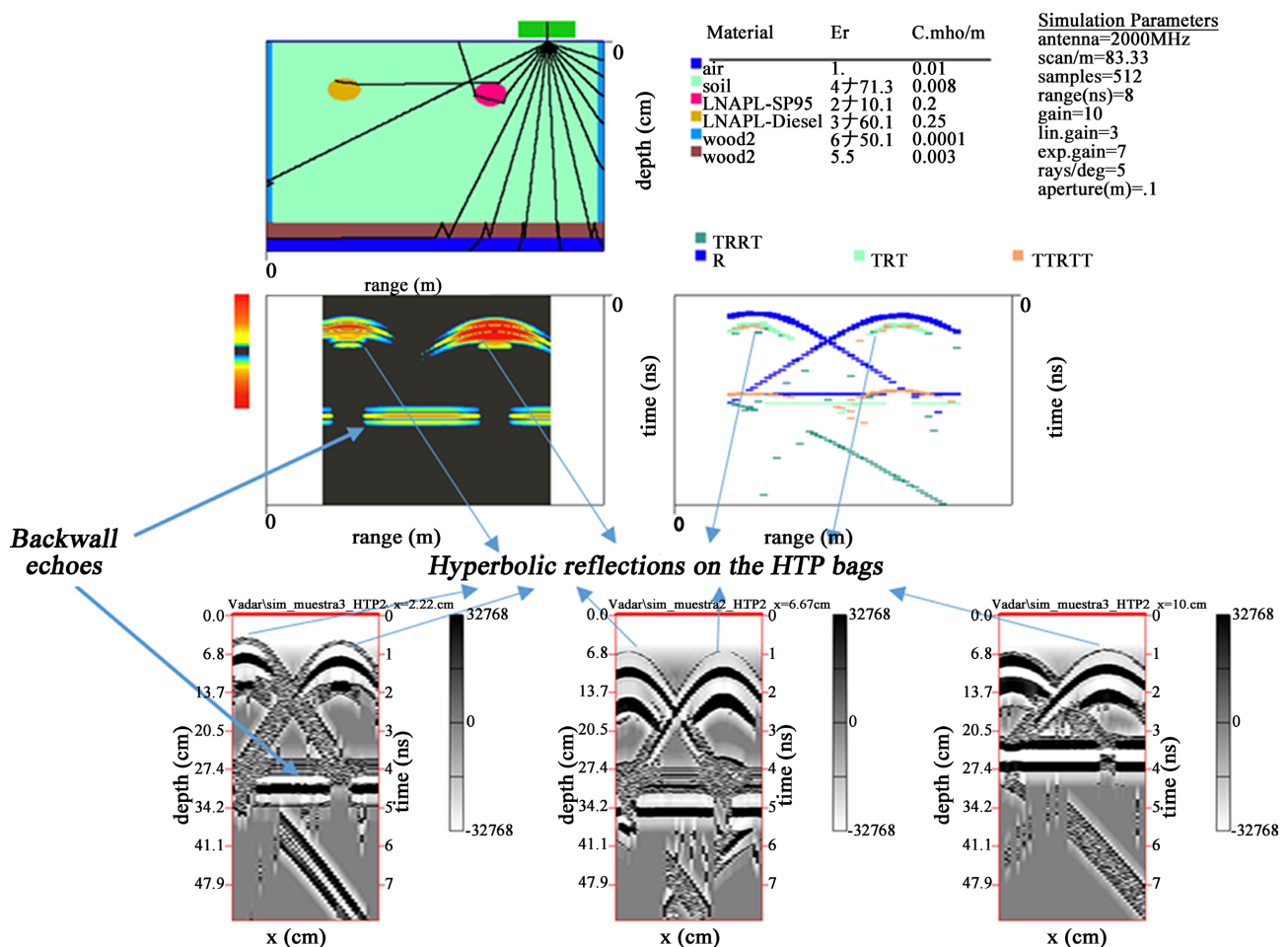


**Figure 3.** Model of geometric sections, dielectric parameters, ray tracing, selected reflection waves and synthetic radargrams obtained by the three soil samples with buried combustible bags.

GPR profiles (static and dynamic pulse/eco mode configuration) using some software tools. The GPR-Slice<sup>®</sup> is used to get the reset to zero-time using the 15% threshold method and the wave arrival of some interested reflection mainly back-wall echo on the bottom and hyperbolic reflection in the plastic bags. Also, it was also used to extract some signal parameters in the time and frequency domain as follows:

- Maximum frequency (MFQ in Hertz, Hz) measured in the time-frequency transform of individual traces. The time-frequency distribution (TFD) is a 2D-map where axis are time (or depth) and frequency and the values are related with amplitude or energy of the signal or traces. For one single trace, one TFD is obtained while it is required a lot of traces to obtain one radargram. To obtain the time-frequency representation the S-transform based on continuous wavelet transform CWT  $W(t, d)$  of a giving function  $h(t)$ , is used, where  $d$  is a dilation time that control resolution between time and spectra according to:

$$W(\tau, d) = \int_{-\infty}^{\infty} h(t) \cdot w(t - \tau, d) dt \quad (2)$$

where the  $w(t, \tau)$  is a scaled replica of the fundamental decomposition of the mother wavelet. Therefore, the S-transform in time and frequency domain of the above giving trace  $h(t)$  is defined by the multiplied phase factor (Stockwell et al., 1996):

$$S(t, f) = e^{i2\pi f t} \cdot W(\tau, d) \quad (3)$$

The exponential-decay law curve fitting curve allows to calculate de attenuation coefficient (ATC) in terms of nepers/ns. This time domain attribute is calculated after the zero-time correction and the first echo arrival with the same length for each set of signals.

- The instantaneous amplitude (IAM) (in arbitrary units) is calculated from the analytic signal and it is related with the reflectivity strength, reducing the random appearance of the signal in the radargram that it is very convenient on data with several reflections. Next **Figure 4** shows the three main representations calculated by above describe methods.

### 3. GPR Analysis and Results

In this section, the main results from the experiments carried out in the lab-scaled soil specimens along with the synthetic radargrams obtained by numerical simulation are shown. In order to find some evidence about the best signal attributes to detect and locate the presence of hydrocarbons, before going to the field measurements, the results are analyzed.

#### 3.1. Electric/Dielectric Characterization of the Soil Samples

The basic electrical parameters that define electrical and dielectric behavior of soils are dc-electrical conductivity and dielectric permittivity. These properties are strongly influenced by porosity and WC of the soil samples.

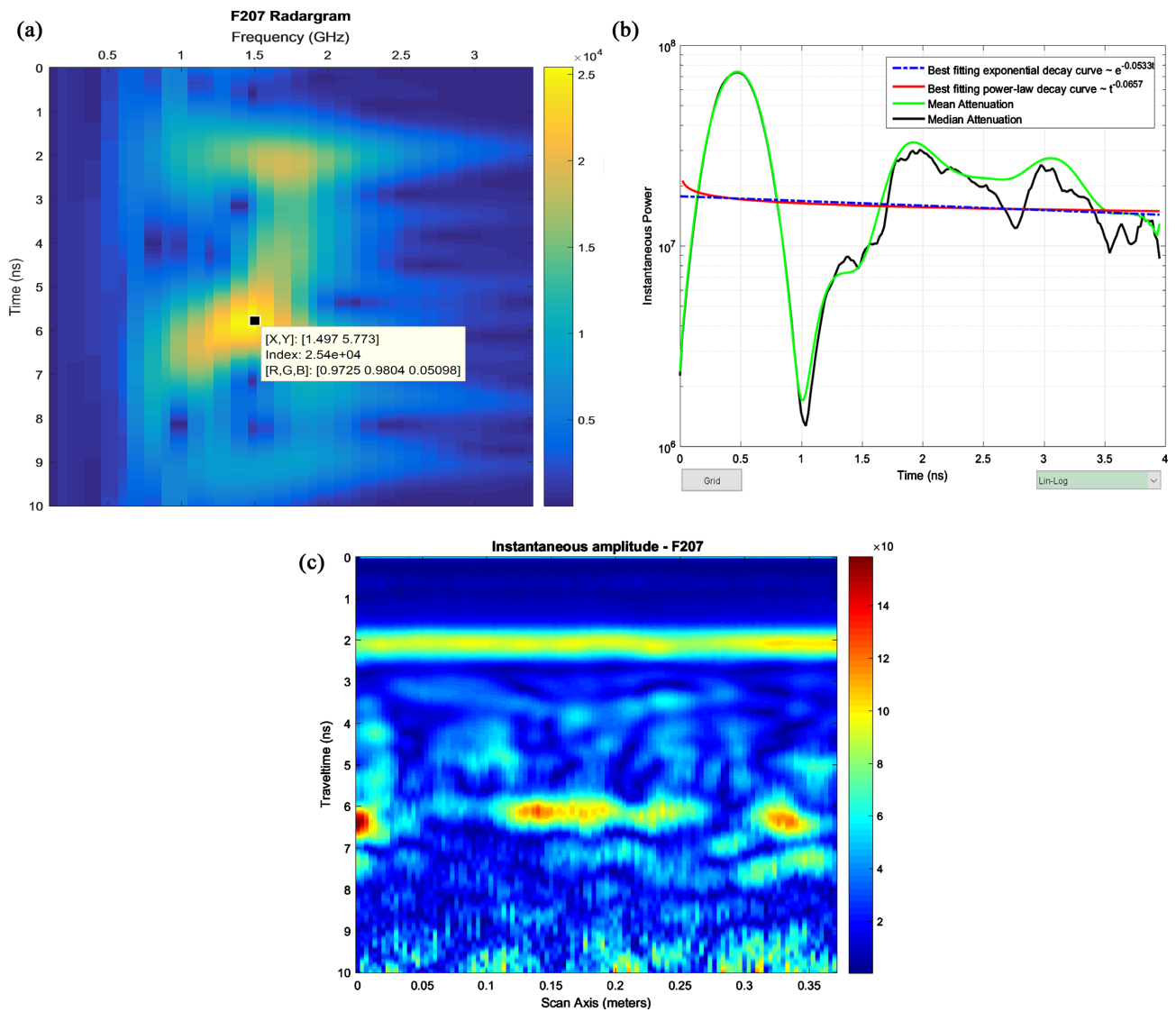


**Figure 4.** Time and frequency domain signal attribute representation: (a) Maximum frequency at the spectrogram calculated in a single GPR trace; (b) Attenuation coefficient (ATC) modeling in time domain; (c) Instantaneous amplitude (IAM) representation equivalent to typical radargram.

DC-electrical conductivity was measured by Wenner configuration of 4 electrodes using Syscal R1+ resistivity meter of the IRIS® brand. The averaged measured conductivities for soil samples at the initial conditions (round 1 and thickness T3) were the following: a) 1.90, b) 2.92 and c) 3.75 mS/m for samples S1, S2 and S3 respectively, which are in the range of the mixtures reported by F.J. Moreno [15]. As the time goes on a drying effect appeared and a decreasing of electrical conductivity at the round 2 to values of: i) 1.90, ii) 2.73 and iii) 1.15 mS/m.

By the other hand, regarding the estimation of dielectric permittivity, it is known that the time of flight (calculating the depth according the 2-way travel) and wave or phase velocity are directly related and the velocity and dielectric constant has a simple translation through Equation (1). The time of flight was

measured as the difference between corrected zero-time and the time corresponding the sample on which the signal rapid changes by the wave arrival from the bottom reflection or the buried LHB targets. The correspondence between depth and time of flight is set by the velocity. Adopting a 1D-model velocity, it is calculated by curve fitting on the buried narrow cylindrical tubes shown in **Figure 2(a)** and the fitting hyperbola in next **Figure 5(a)**. The migration process is a correction of the signal diffraction and it is used to recuperate the real shape and size of the buried target.

Next **Table 3** shows the calculated velocities and dielectric constant derived from the fitting hyperbolic reflections of known targets.

An increasing of velocity and the correspondence decreasing of dielectric

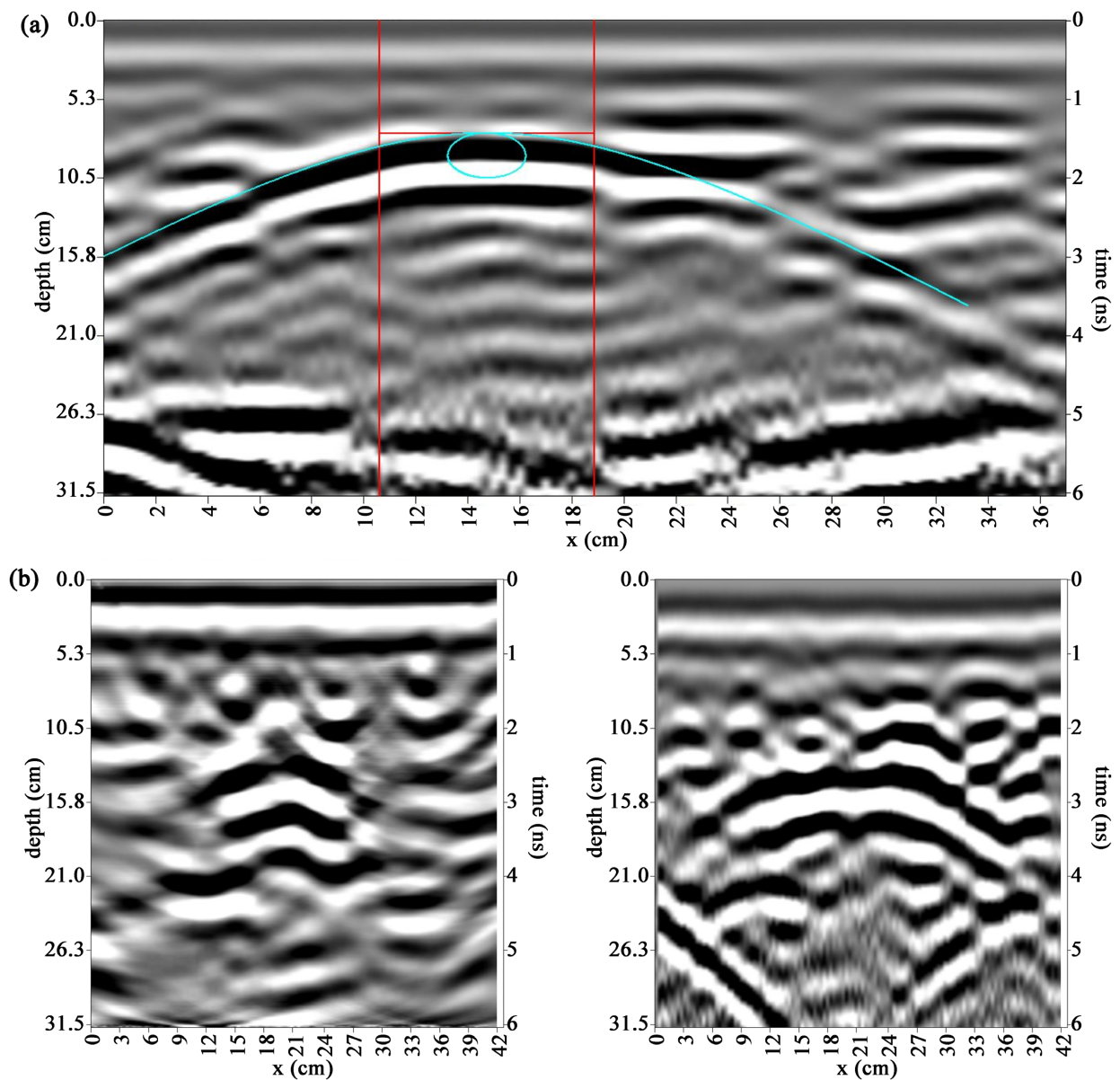


**Figure 5.** (a) Hyperbolic fitting process and (b) migrated and bandpass filter radargrams for the S2. The LHB top was placed at 68 mm. in depth.

constant  $\epsilon$  is observed from round 2 respecting the initial round 1.

The dielectric constants were measured for a range of known bottom depths respect to the antenna position from the three different sample thicknesses and for the three working frequencies. The results are in **Table 4**.

At first sight, the dielectric behavior does not show any trend but selecting those values that correspond to measurement with appropriate resolution in terms of wavelength and propagated length, could be found a slight downward trend with the frequency. The selected values\* will avoid the short depth and low frequencies where the wavelength are in the range of propagation depth. The following data (270 MHz-T<sub>1</sub> and T<sub>2</sub>, 900 MHz-T<sub>1</sub>) were not considered.

Next **Figure 6** allows the observation of a linear decreasing trend.

According to the electrical conductivity ranges of each soil sample, it can be known dispersion of the electromagnetic signal through the specimen would be present. In wide materials and frequency ranges the wave velocity calculation approaches to the simple Equation (1). Most linear decreasing has been found for the three soil samples and the thickness T3, but low slope values has been found. In the doctoral research work of V. Perez-Gracia (*Perez-Gracia, 2001*) there are some groups of plots for the velocity dispersion (velocity vs frequency) regarding different electrical conductivities. Comparing the dc-electrical conductivities measured and the working frequencies, it can be concluded that the

**Table 3.** Wave velocity (v) and dielectric constant ( $\epsilon$ ) at the frequency of 2 GHz (v/ $\epsilon$ ) and associated wavelength ( $\lambda$ ) to the used frequencies.

Samples	Round 1			Round 2				
	Velocity (mm/ns) fitted curve	$\lambda$ Wavelength (mm)			Velocity (mm/ns) fitted curve	$\lambda$ Wavelength (mm)		
	2 GHz/ $\epsilon$	270	900	2000	2 GHz/ $\epsilon$	270	900	2000
Soil 1	080/14.06	29.6	8.9	4.1	137/4.78	50.7	15.2	6.8
Soil 2	108/8.06	40.0	12.0	5.4	118/6.78	43.7	13.1	5.9
Soil 3	118/6.49	43.7	13.1	5.9	168/3.20	62.2	18.6	8.4

**Table 4.** Dielectric constant  $\epsilon$  at the thickness T<sub>i</sub>, median and standard deviation (SD) in the round 1.

Round 1 Samples	Sample 1			Sample 2			Sample 3		
	T1	T2	T3	T1	T2	T3	T1	T2	T3
270	11.0	13.6	14.6	8.0	8.4	8.6	5.6	3.2	6.5
900	14.3	14.1	14.5	7.6	8.3	7.1	8.7	7.5	6.0
2000	14.4	14.2	13.2	8.1	8.1	6.7	6.7	6.8	5.8
Median $\epsilon \pm$ SD	13.8 $\pm$ 1.1			7.9 $\pm$ 0.6			6.3 $\pm$ 1.0		
Selected values* Median $\epsilon \pm$ SD	14.2 $\pm$ 0.4			7.8 $\pm$ 0.7			6.5 $\pm$ 0.4		

controlled experiments are not affected by the dispersion effect which could appears at lower frequencies from 50 MHz.

Next **Figure 7** shows how matches the measured dielectric constant  $\epsilon$  at both testing rounds framed in a plot representation for similar materials as silica sand, Vernon loam, clay mixture and clayed sand. In this sense, silica sand and

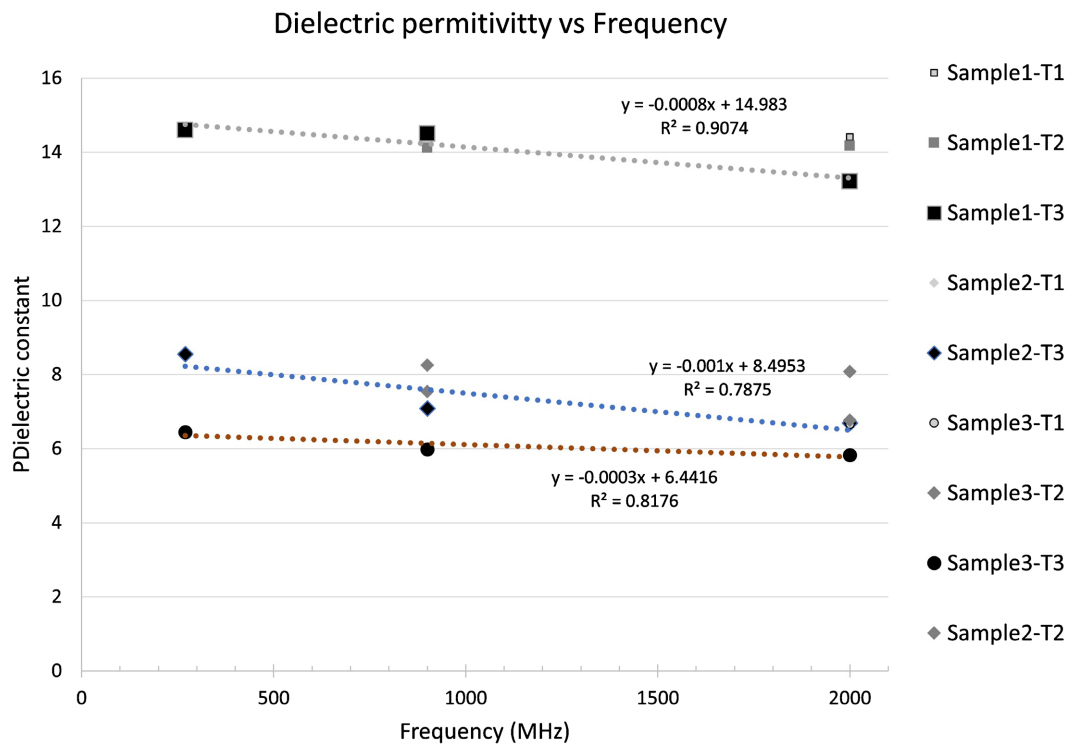


**Figure 6.** Dielectric constant values by thickness and working frequency.

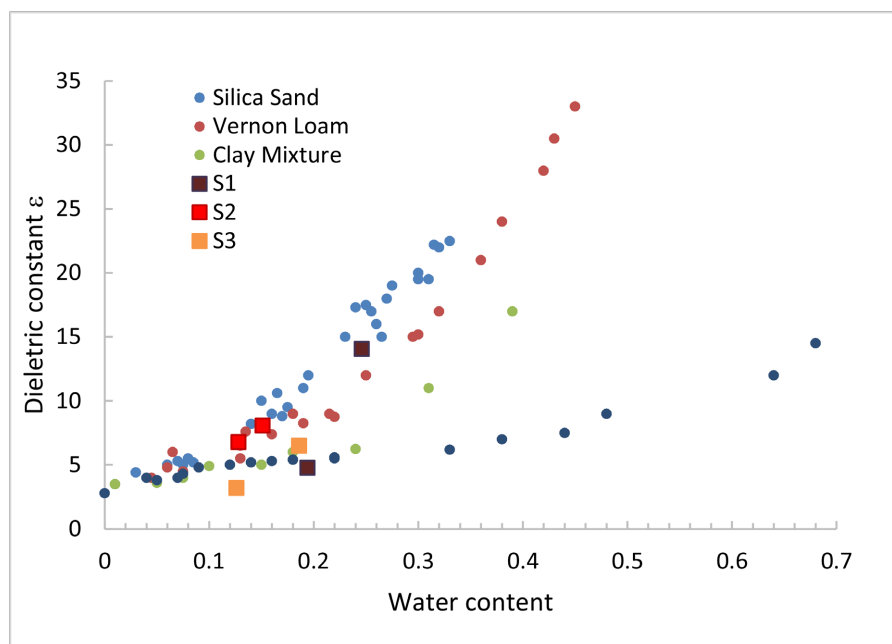


**Figure 7.** Dielectric constant versus water content for referenced and tested samples  $S_i$ .

clayed sand (0.35% weight clay content) would be drawn to be compared with S3. Loamy soil is plotted to be compared with S1 and clay mixture would be compared with S2. The referenced soils were taken from Knoll (Knoll, 1996).

The estimates for the dielectric constant of S1 sample matches partially with an example of Vermont loam soil from the referenced work. The estimate for round 2 shows lower values than expected that could be explained by the presence of gravels that can determine the dielectric behavior when the free water is reduced. The change found in the dielectric constant  $\epsilon$  was reported by Knoll (Knoll, 1996).

for the expected dielectric permittivity evolution ranges when the porosity increases, by using relationship for the low clays contains and loamy soil as the case of S1, when an important decreasing value has been observed and that is what it has been measured from 14.06 to 4.78.

For the clay sample S2, it is observed small decreasing water content (WC) and slight increasing of porosity so that the sample conditions remain quite constant. For the referenced work of Knoll (Knoll, 1996) and (Knoll & Knight, 1994), the high content of clayed materials does not show relevant changes at the dielectric constant according to the experimental obtained values from round 1 (7.8) to round 2 (6.8). To see greater changes, the water content should be around of 60% - 70% in clayed materials as reveals figure 6.5 of the referenced work (Perez-Gracia, 2001) that it is far from lab conditions.

For the S3, it can be noticed the low electrical conductivity for sandy materials (0.9 mS/m) while there is observed a great increasing in open porosity from 0.35 to 0.5 reveals the absorption capacity due to the high specific particle surface. The observed decrease in  $\epsilon$  from 6.5 to 3.2 is coherent with the high increment in open porosity and predicted by M. D. Knoll (Knoll, 1996) at page 138 (mixture sand and clay-kaolinite), finding that the best fit if it is considered some clay addition and not strictly dry for S3.

By the other hand, the attenuation coefficient measured by fitting exponential decay model was calculated for the 2-way propagation corresponding soil samples including the interface echo (initial) and the just before the backwall echo from the basement arrivals.

**Table 5** shows the results for the attenuation coefficient applying an exponential decay model between 2-way travel avoiding the influence of the backwall reflection when dielectric contrast would disturbs range of data shiftment between round tests. It is noticed that sample 1 and 3 decrease around 1 dB/ns

**Table 5.** Median attenuation coefficients in both round tests for the HWF (2 GHz) and  $T_2$ .

Samples	Round 1 $\alpha$ (dB/ns)	Round 2 $\alpha$ (dB/ns)
Soil 1	14.76	12.84
Soil 2	12.24	2.31
Soil 3	14.99	14.15

while high content clay affects to the signal attenuation stronger than the other kind of samples showing a potential decrease around of 10 dB/ns.

These values were used as an input for the numerical simulations.

### 3.2. Dielectric Characterization of the LNAPL

Some buried plastic bags filled with diesel and gasoline (LHB) were tested before and after being buried in the correspondent soil sample at final conditions (Round 2). Some preliminary GPR measurements were done with the next results in **Table 6** (see **Table 2(d)**). The results also confirm what is found in the literature review because great part of the hydrocarbon substances are in the range of 1 - 5 of their dielectric permittivity. These values should be verified in the GPR measurements for the buried plastic bags.

The vertical accuracy is frequently compared with the  $\lambda/4$  of the GPR wave. The round 2 aimed to assess the detection and sizing abilities for GPR methodology in this environment (controlled experiments) was performed transversal and longitudinal profiles crossing the buried plastic bags around 5 - 10 cm of depth using HWF of 2 GHz antenna. Some schematic configurations were shown in **Figure 3** (tracing geometry). The type of analysis was described in subsection 2.3 and specially it is enhanced the described signal attributes as the instantaneous amplitude (IAM) and the spectral shiftment of the maximum frequency (MFQ) in the TFD calculated in the analytic signal to find some evidence of the more influence at the spectral response than the temporal evolution of the electromagnetic wave exerted by the hydrocarbon presence.

In the radargrams of **Figure 8** it was measured the arrival time in the top hyperbola reflection at the bag sections, the complex measuring of reflection on the bag bottom and the possible changes on the backwall echo at the box basement aligned to the bag LNAPL targets.

Next **Table 7** summarizes the main achieved results, calling  $\Delta_{top}$  the depth deviation between real and measured depth of the bag (diesel and gasoline), dielectric constant  $\epsilon$  of diesel and gasoline calculated from the top-bottom bag reflection.

The values in **Table 7** show that it is producing a constant shiftment in the depth determination of the bag top ranged between 0.6 - 2.0 mm. Sandy soil shows greater oscillations between testing rounds even overestimation in case of

**Table 6.** Dielectric LNAPL plastic bags (LHB) characterization.

	Diesel	Gasoline
Depth or Vertical Size (mm)	31	42
Time of flight (ns)	0.391	0.390
Dielectric permittivity $\epsilon$	3.60	1.95
Velocity (mm/ns)	159	215
$\lambda/4$ (mm)	19.7	27

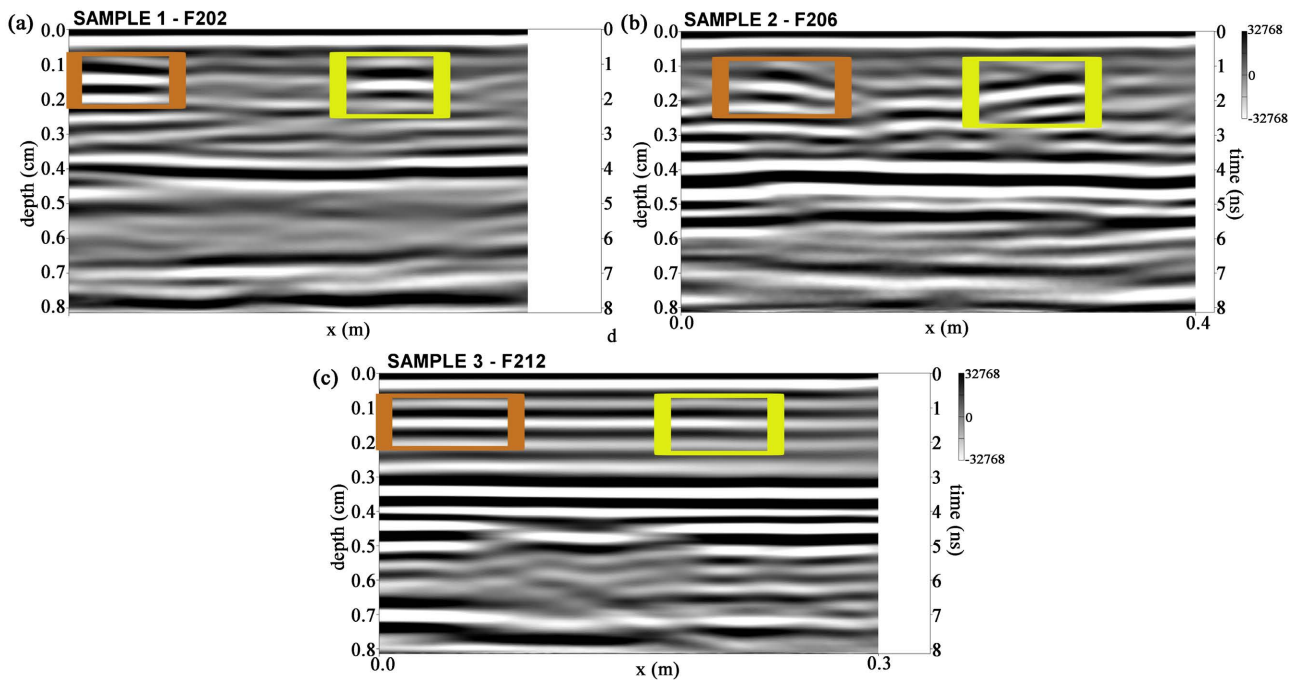


**Figure 8.** Migrated radargram for its specific velocity for (a) Soil sample 1; (b) Soil sample 2; (c) Soil sample 3. BCBs presented by dashed-coloured bags (yellow-gasoline and brown-diesel) and cursor points for the time calculation.

**Table 7.** Dielectric constant  $\epsilon$  (mean and standard deviation SD).

Rounds Parameters/Samples	Round1			Round2		
	S1	S2	S3	S1	S2	S3
$\Delta_{top}$ (mm)	1.2	2.0	0.6	1.1	1.5	-2.1
$\epsilon_{air}$	1.3	1.3	-	-	-	-
$\epsilon_{diesel} (\pm\sigma)$	$3.7 \pm 0.8$	$2.5 \pm 0.7$	3.8	$2.7 \pm 0.9$	5.1	$3.2 \pm 0.1$
$\epsilon_{gasoline} (\pm\sigma)$	1.95	$1.9 \pm 0.3$	$2.3 \pm 0.7$	$1.9 \pm 0.2$	3.2	$2.9 \pm 0.6$
$\epsilon_{diesel} (\pm\sigma)$ (ref. value)	$3.2 \pm 0.9$ (3.6)			$2.9 \pm 0.7$ (3.6)		
$\epsilon_{gasoline} (\pm\sigma)$ (ref.)	$2.4 \pm 0.8$ (1.95)			$2.5 \pm 0.6$ (1.95)		

round 2 when sand particles are drier than the round 1 aiming at some diverse local velocities than the overall velocity adopted for the calculation. Slight lower velocity than 0.3 m/ns was measured for empty space ( $\epsilon_{air}$ ) but near than the unit 1 that it is the expected value.

On the other hand, the dielectric constant values were found in the expected range, producing slight less values for the diesel and high values for gasoline, than measured reference values shown in **Table 6**. The soil S1 produces good estimates for both dielectric constant at both round tests.

To delimit the bag shape the instantaneous amplitude (IAM) revealed as the best attribute for radargrams allowing to determine the thickness and length of the layer in most cases as soil sample 1 at the correspondent section as it can be shown in **Figure 9**.

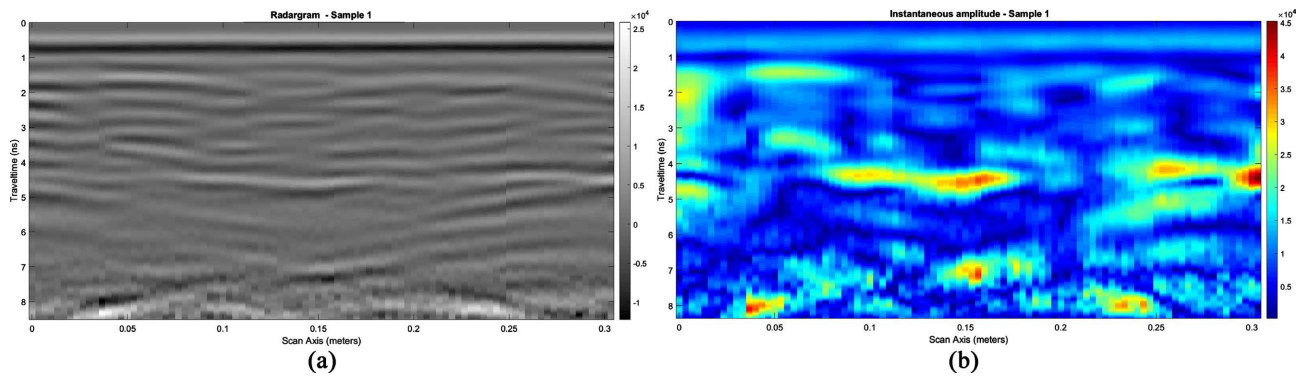


**Figure 9.** Conventional radargram and instantaneous amplitude (IAM) radargram with data markers in the reflections of the LNAPL bag limits and backwall basement of box.

However, the size cannot be measured directly from the axis depth using a 1D-model. It would be corrected according to the following expression for new velocity of the bag content, it means, the hydrocarbon:

$$v_{\text{LNAPL}} = \frac{\text{thick} \cdot 2 \cdot v_{\text{soil}}}{\text{thick} \cdot 2 - \Delta t \cdot v_{\text{soil}}} \quad (4)$$

where  $\Delta t$  is the time between top and bottom depths for the indicated high instantaneous amplitude,  $v_{\text{soil}}$  is the soil sample velocity measured by fitting hyperbolic curve or by the time of the backwall reflection.

### 3.3. Time and Frequency Behavior of the LNAPL on Controlled Experiments

Another valuable attribute to detect the presence of LNAPL is the maximum frequency (MFQ) and its shiftment that can be easily located using a set of a TFD for each GPR trace as it is described in the previous section and showed in **Figure 4(a)**.

In **Figure 10**, the maximum frequencies for the correspondent traces equally separated for the total length of GPR profile (40 cm), performed with the HWF 2 GHz (round 2) were showed. The straight brown line represents the maximum frequency in absence of LNAPL plastic bags so that it could be considered as the reference level. The red circular points belong to MFQ of a GPR profile that crosses transversally the bags and their orientative location are shown by the quasi-circular shape (orange for diesel and yellow for the gasoline). The diamond data belongs to longitudinal profiles where the plastic bag reflection are shown as eccentric ovals. It was found some shiftments in the expected frequency when the trace is aligned with an hydrocarbon plastic bags (LHB) in depth confirming the effect of the LNAPL into the spectral response of the GPR signal. This effect consists of a decrease of the maximum frequency (MFQ) on the TFD, clearly observed in the clay soil (sample S2), partially observed for the gasoline case for the sample S1 and the effect is not observed for the sandy soil (sample S3).

### 3.4. Characterization of the Attributes on Synthetic Radargrams

The numerical simulations aim to confirm the experimental results. Some pre-

liminar parameters were used as inputs to build up the models. It was simulated 40 cm of scan profiles for the considered soil sample, geometries of the wooden box and the size and location to the ground level of LNAPL plastic bags. Apart from the electrical conductivity for each soil, velocities in m/ns and attenuation in dB/ns were used as a reference and fitting the dielectric permittivity as complex value to match as possible the experimental values.

The radargrams of **Figure 11** correspond to profiles with absence of the NAPL plastic bags and the below radargrams with diesel and gasoline bags inside in depth where simulates as the transversal GPR profiles. The echoes from backwall (bottom) show uniform reflections with some small changes. The plastic bag shapes are well recuperated except the bottom part in case of sandy soil (sample S3). Finally, the time frequency analysis provides the same shift effect on the maximum frequency on traces with the plastic bags filled with hydrocarbon.

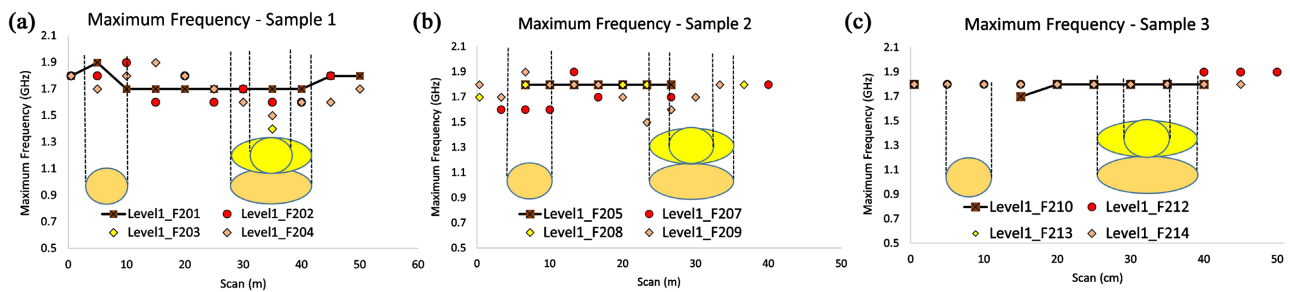


**Figure 10.** Estimated MFQ from the time-frequency diagrams for the soil samples: (a) Soil 1 (b) Soil 2 and (c) Soil 3, all of three with both the LHB.

**Table 8.** Complex dielectric constant  $\epsilon$ , attenuation coefficient, wave velocity and dc-conductivity.

Samples	$\epsilon_{real}/\epsilon_{imag}$	$\alpha$ (dB/ns)	Velocity (cm/ns)	$\sigma$ (mS/m)
Soil 1	4.73/1.3	13.07	13.65 (13.7)	1.09
Soil 2	5.3/0.35	43.80	11.86 (11.8)	2.73
Soil 3	3.35/1.3	14.91	16.89 (16.8)	1.15

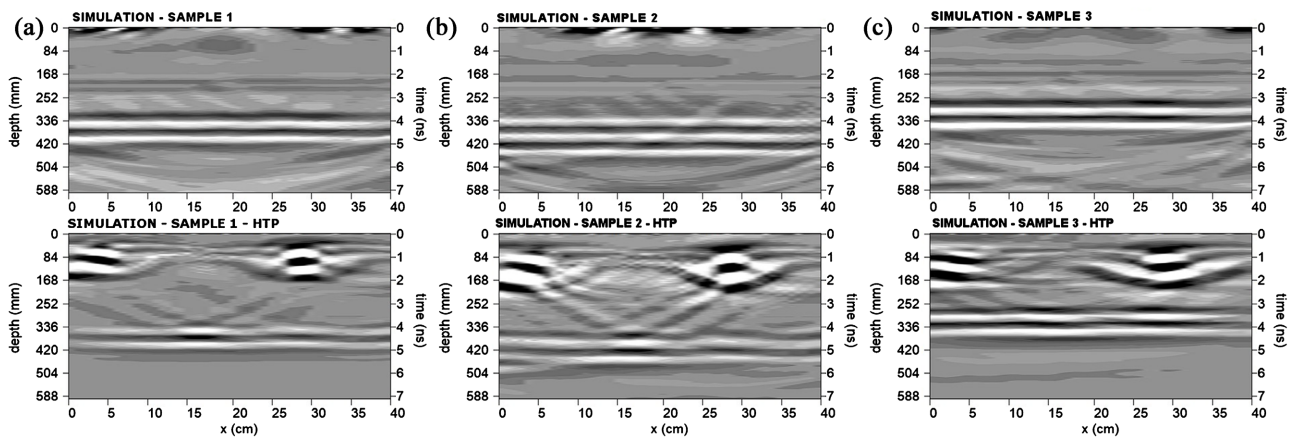


**Figure 11.** Migrated Radargrams for soil sample S1 (a), soil sample S2 (b) and soil sample S3 (c).

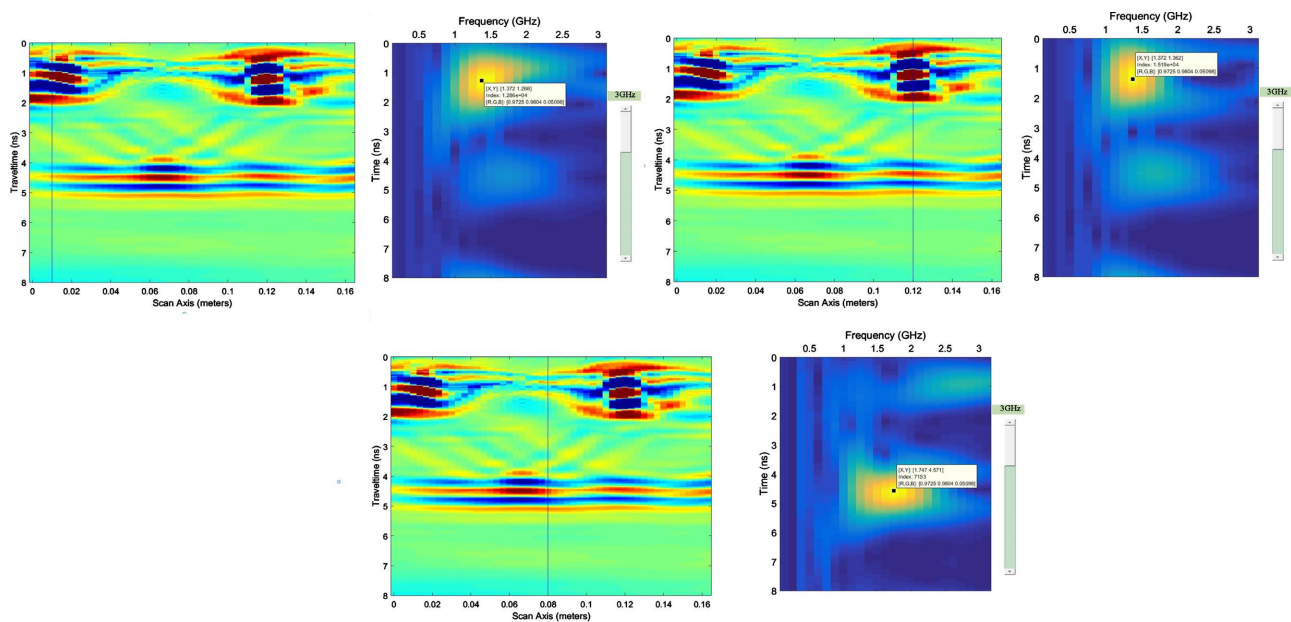


**Figure 12.** Synthetic radargram with migration correction and time-frequency distribution with indicated maximum frequency (MFQ).

In **Figure 12**, three traces have been selected belonging to diesel bag (left), gasoline bag (right) and no-bag position (low) indicated with a vertical line in the synthetic radargram. At the right side of each synthetic radargram are shown the time-frequency ranged in the energy received in pulse/echo allow determining the frequency of the maximum return energy. It is shown that the gasoline with lower dielectric permittivity produces the most readable shiftment with a decreasing value of the MFQ from the typical values for not aligned traces to the LHB.

#### 4. Conclusion

The dielectric permittivity  $\epsilon$  evolution from environmental conditions with a high percentage of water absorption range of soil sample (round 1) and stored conditions (not dry) at laboratory premises (round 2) has been analyzed and it contrasts with the expected evolution for clay and sandy mixtures reported in the literature review. It is found that measured dielectric constant ranges and changes are in coherence with the complimentary test as open porosity and water content change. The natural soil with low clay content reveals a high decreasing effect conducted by the water presence reduction in opposite as clay sample which slight decreasing is observed in accordance with the previous accuracy laboratory experiments. The sandy soil dielectric constant shifts to the typical dry values.

In that context, it is conducted some characterization of potential LNAPL contaminant confined and not dissolved or diffused in the soil samples so that it is not activated the expected chemical reactions of biodegradation. The 2 GHz working frequency has allowed the dielectric constant estimation that ranges reported in the literature review. Some simple experiments have been led to

detect and size buried plastic bags filled with diesel and gasoline substances. Typical amplitude of migrated radargrams, instantaneous amplitude of migrated radargrams and time-frequency distributions have been analyzed to observe the behavior of the specific signal attribute in the LNAPL substance presence.

The detection is produced in all the soil samples with the hyperbola reflection of buried bags but it is more detectable when the dielectric constant is higher. The best case is for sample 1 and sample 2 and the worst case is for the sandy soil 3 in round 2 where its dielectric constant value 3.2 is close to the dielectric values of the LNAPL substance.

The size in the depth of the buried bags was measured by the instantaneous amplitude of the migrated radargrams much better than with the typical amplitude of the correspondent migrated radargrams. Therefore, it is important to know the average velocity of the predominant soil.

Time-frequency distributions were used to estimate the frequency of the maximum energy to obtain the frequency shift as a parameter to find the possible presence of LNAPL substance.

Based on these achievements, an on-site GPR survey will undertake to explore the expectation of the real application regretting the difficulty to get access to a well-known subsoil characterization on a contaminated area.

## Acknowledgements

This research was funded by Programa Torres-Quevedo of the Spanish Ministerio de Ciencia e Innovación, grant number PTQ-17-09251.

## Conflicts of Interest

The authors declare no conflicts of interest regarding the publication of this paper.

## References

- Carcione, J. M., & Seriani, G. (2000). An Electromagnetic Modelling Tool for the Detection of Hydrocarbons in the Subsoil. *Geophysical Prospecting*, *48*, 231-256. <https://doi.org/10.1046/j.1365-2478.2000.00187.x>
- Che-Alota, V., Atekwana, E. A., Sauck, W. A., & Werkema, D. D. (2009). Temporal Geophysical Signatures from Contaminant-Mass Remediation. *Geophysics*, *4*, 113-123. <https://doi.org/10.1190/1.3139769>
- Chen, H., Kang, J., Chen, Y., Xu, D., & Hu, Y. (2017). An Improved Time-Frequency Analysis Method for Hydrocarbon Detection Based on EWT and SET. *Energies*, *10*, Article No. 1090. <https://doi.org/10.3390/en10081090>
- Chen, H. W., Fan, C. C., Chen, S. Y., & Lu, C. M. (2012). Detection and Analysis of LNAPL Contaminated Site by Integrated Time-Lapse GPR Surveys. In *14th International Conference on Ground Penetrating Radar (GPR)* (pp. 764-768). IEEE. <https://doi.org/10.1109/ICGPR.2012.6254964>
- Capozzoli, L., Giampaolo, V., Rizzo, E., Votta, M., Cucci, P. L., & De Biase, M. et al. (2012). Ground Penetrating Radar as a Powerful Tool for the Study and the Monitoring of LNAPL-Contamination in the Subsoil. In *Proceedings of the 31st Convegno Gruppo*

*Nazionale Geofisica Terra Solida* (pp. 60-67).

- Deceuster, J., & Kaufmann, O. (2012). Improving the Delineation of Hydrocarbon-Impacted Soils and Water through Induced Polarization (IP) Tomographies: A Field Study at an Industrial Waste Land. *Journal of Contaminant Hydrology*, 136-137, 25-42. <https://doi.org/10.1016/j.jconhyd.2012.05.003>
- Golebiowski, T., Tomecka-Suchoń, S., Marcak, H., & Zogola, B. (2010). Aiding of the GPR Method by Other Measurement Techniques for Liquid Contamination Detection. In *Proceedings of the XIII International Conference on Ground Penetrating Radar* (pp.1-6). IEEE. <https://doi.org/10.1109/ICGPR.2010.5550160>  
[https://www.researchgate.net/publication/251946572\\_Aiding\\_of\\_the\\_GPR\\_method\\_by\\_other\\_measurement\\_techniques\\_for\\_liquid\\_contamination\\_detection](https://www.researchgate.net/publication/251946572_Aiding_of_the_GPR_method_by_other_measurement_techniques_for_liquid_contamination_detection)
- Hamzah, U., Ismail, M. A., & Samsudin, A. R. (2008). Geophysical Techniques in the Study of Hydrocarbon-Contaminated Soil. *Bulletin of the Geological Society of Malaysia*, 54, 133-138.
- Rial, F. I., Pereira, M., Lorenzo, H., Arias, P., & Novo, A. (2007). Vertical and Horizontal Resolution of GPR Bow-Tie Antennas. In *4th International Workshop on, Advanced Ground Penetrating Radar* (pp. 187-191). IEEE. <https://doi.org/10.1109/AGPR.2007.386549>
- Jiang, Y., Li, Y., Yang, G., Zhou, X., Wu, J., & Shi, X. (2013). The Application of High-Density Resistivity Method in Organic Pollution Survey of Groundwater and Soil. *Procedia Earth and Planetary Science*, 7, 932-935. <https://doi.org/10.1016/j.proeps.2013.03.011>
- Knoll, M. D., & Knight, R. (1994). Relationships between Dielectric and Hydrogeologic Properties of Sand-Clay Mixtures. In *Fifth International Conference on Ground Penetrating Radar* (pp. 45-61). European Association of Geoscientists & Engineers. <https://doi.org/10.3997/2214-4609-pdb.300.4>
- Knoll, M. D. (1996). *A Petrophysical for GPR and Very Early Time of Electromagnetics: Electrical Properties of Sand-Clay Mixtures*. Ph.D. Thesis, Faculty of Graduated Sciences, Dpt. of Science on Earth and Ocean Sciences, University of British Columbia.
- Orlando, L. (2002). Detection and Analysis of LNAPL Using the Instantaneous Amplitude and Frequency of Ground-Penetrating Radar Data. *Geophysical Prospecting*, 50, 27-41. <https://doi.org/10.1046/j.1365-2478.2002.00288.x>
- Mansi, A. H., Castillo, M. P., & Bernasconi, G. (2017). Controlled Laboratory Test for the Investigation of LNAPL Contamination Using a 2.0 GHz Ground Penetrating Radar. *Bollettino di Geofisica Teorica ed Applicata*, 58, 169-180.
- Marcak, H. & Gołębowski, T. (2008). Changes of GPR Spectra Due to the Presence of Hydrocarbon Contamination in the Ground. *Acta Geophysica*, 56, Article No. 485. <https://doi.org/10.2478/s11600-008-0003-4>
- McCallister, J. T. (1994). *Experiment to Test Ground Penetrating Radar for Gasoline Detection*. Degree of Bachelor of Science in Geology and Mineralogy, Ohio State University.
- Moreno, F. J., & Montes, L.A (2003). Caracterización de depósitos de suelo utilizando geo-radar. *Geofísica Colombiana*, No. 7, 42-48.
- Pérez-Gracia, V. (2001). Radar de subsuelo. Evaluación para aplicaciones en arqueología y en patrimonio histórico-artístico. *Chapters 4 & 6. Dpto. Ingeniería del Terreno, Cartografía y Geofísica*. Tesis Doctoral, Universitat Politècnica de Catalunya.
- Shamir, O., Goldshleger, N., Basson, U., & Reshef, M. (2018). Laboratory Measurements of Subsurface Spatial. Moisture Content by Ground-Penetrating Radar (GPR) Diffraction

- tion and Reflection Imaging of Agricultural Soils. *Remote Sensing*, 10, Article No. 1667. <https://doi.org/10.3390/rs10101667>
- Sogade, J. A., Scira-Scappuzzo, F., Vichabian, Y., Shi, W., Rodi, W., Lesmes, D. P. et al. (2006). Induced-Polarization Detection and Mapping of Contaminant Plumes. *Geophysics*, 71, 75-84. <https://doi.org/10.1190/1.2196873>
- Stockwell, R. G., Mansinha, L., & Lowe, R. P. (1996). Localization of the Complex Spectrum: The S-Transform. *IEEE Transactions on Signal Processing*, 44, 998-1001. <https://doi.org/10.1109/78.492555>
- Tejero, A., & López, A. E. (2013). El método de polarización inducida aplicado en la contaminación de suelos por hidrocarburos. *Boletín de Sociedad Geológica Mexicana*, 65, 1-8. <https://doi.org/10.18268/BSGM2013v65n1a1>
- Tomás, R., Cano, M., García-Barba, J., Santamarta, J. C., Hernández, J. C., Rodríguez, J. A. et al. (2013). *Prácticas de Ingeniería del Terreno*. Universidades de Alicante y de La Laguna. <http://web.ua.es/es/ginter/>
- Wijewardana, N. S., Galagedara, L. W., & Mowjood, M. I. M. (2012). GprMax2D Modelling to Identify Contaminated Areas in Groundwater with Landfill Leachate. *Annual Research Journal of SLSAJ*, 12, 16-22.